Geochronology, 2, 155–167, 2020
https://doi.org/10.5194/gchron-2-155-2020

GEOCHRONOLOGY Open Access EGU

Evaluating the reliability of U–Pb laser ablation inductively coupled plasma mass spectrometry (LA-ICP-MS) carbonate geochronology: matrix issues and a potential calcite validation reference material

Marcel Guillong, Jörn-Frederik Wotzlaw, Nathan Looser, and Oscar Laurent

Department of Earth Sciences, ETH, Zurich, 8092, Switzerland

Correspondence: Marcel Guillong (guillong@erdw.ethz.ch)

Received: 16 December 2019 – Discussion started: 27 January 2020
Revised: 11 May 2020 – Accepted: 20 May 2020 – Published: 30 June 2020

Abstract. We document that the reliability of carbonate U–Pb dating by laser ablation inductively coupled plasma mass spectrometry (LA-ICP-MS) is improved by matching the aspect ratio of the LA single-hole drilling craters and propagating long-term excess variance and systematic uncertainties. We investigated the impact of different matrices and ablation crater geometries using U–Pb isotope analyses of one primary (WC-1) and two secondary reference materials (RMs). Validation RMs (VRMs) include a previously characterised one (ASH-15D) and a new candidate (JT), characterised by ID-TIMS (intercept age: 13.797 ± 0.031 Ma) with excellent agreement to pooled LA-ICP-MS measurements (13.75 ± 0.11 | 0.36 Ma), a U concentration of approx. 1 µg g^{-1} and $^{238}U/^{206}Pb$ ratios from 5 to 460, defining the isochron well. Differences in ablation crater depth to diameter ratios (aspect ratio) introduce an offset due to downhole fractionation and/or matrix effects. This effect can be observed either when the crater size between U–Pb RM and the sample changes or when the ablation rate for the sample is different than for the RM. Observed deviations are up to 20 % of the final intercept age depending on the degree of crater geometry mismatch. The long-term excess uncertainty was calculated to be in the range of 2 % (ASH-15D) to 2.5 % (JT), and we recommend propagating this uncertainty into the uncertainty of the final results. Additionally, a systematic offset to the ID-TIMS age of 2 %–3 % was observed for ASH-15D but not for JT. This offset might be due to different ablation rates of ASH-15D compared to the primary RM or remaining matrix effects, even when the aspect ratios chosen are similar.

1 Introduction

Recent improvements in the sensitivity of inductively coupled plasma mass spectrometry (ICP-MS) instruments coupled to a laser ablation system allows us to date not only very young zircons by the U–Pb method (Guillong et al., 2014) but also minerals with very low U concentrations, typically of several parts per billion to tens of parts per million and even lower concentrations of radiogenic Pb, such as carbonates (Li et al., 2014; Methner et al., 2016; Roberts and Walker, 2016; Nuriel et al., 2017). Additionally, carbonates often incorporate variable amounts of initial (common) Pb during crystallisation from aqueous fluids, so that age determination relies on the use of regression lines (isochrons) in the Tera–Wasserburg isotopic space ($^{207}Pb/^{206}Pb$ vs. $^{238}U/^{206}Pb$) (Li et al., 2014). Importantly, this also entails that there is no available carbonate reference material (RM) yielding a concordant U–Pb age. Therefore, accurate U–Pb dating of carbonates requires a two-step data reduction approach (Roberts et al., 2017) consisting of (1) $^{207}Pb/^{206}Pb$ mass bias correction based on a homogeneous reference material (typically a standard glass) and (2) a U/Pb inter-element fractionation correction based on the lower intercept in the Tera–Wasserburg concordia diagram using a matrix-matched RM. With this method, carbonates can be dated by laser ablation ICP-MS (LA-ICP-MS) with the advantage of easy availability, high sample throughput and high spatial resolution, allowing us to resolve large differences in U–Pb ratio and cost effectiveness. Within a day, 300–600 single points can be analysed and a minimum number of 20–30 points per sam-

ple is suggested (Beaudoin et al., 2018; Godeau et al., 2018; Yokoyama et al., 2018), although the appropriate number is strongly sample-specific and depends on the variability of the initial to radiogenic Pb ratios. To maximise the variation in the initial to radiogenic Pb ratios and improve the isochron, new approaches in the acquisition of data by imaging and data pooling were introduced and look promising (Drost et al., 2018).

Previous studies of dating carbonates, mostly calcite, focused either directly on the analytical method development (Li et al., 2014; Roberts et al., 2017; Drost et al., 2018; Yokoyama et al., 2018) or a range of applications from dating fault activity to constraining the timing of hydrothermal mineralisation to directly dating early diagenetic cements in ammonites (Coogan et al., 2016; Methner et al., 2016; Burisch et al., 2017, 2018; Drake et al., 2017; Goodfellow et al., 2017; Nuriel et al., 2017; Hellwig et al., 2018; Walter et al., 2018; MacDonald et al., 2019; Scardia et al., 2019). Only recently, validation RMs (VRMs) have been routinely analysed (e.g. Beaudoin et al., 2018) with data reporting standards following the community-derived standards suggested for zircons (Horstwood et al., 2016). However, no actual data on the long-term excess variance (ε') is given as not many VRMs are available and as the number of sessions including these was limited (Beaudoin et al., 2018). In this work, we introduce a new VRM and aim to investigate the long-term excess variance of U–Pb LA-ICP-MS carbonate dates. In addition, we investigate potential matrix effects influencing the accuracy of such dates, which have been largely overlooked so far. In particular, we document that changes in laser crater aspect ratios between primary RMs and samples may result in significant inaccuracy of U–Pb LA-ICP-MS carbonate dates and propose new analytical strategies to minimise this effect.

2 Instrumentation, methods and samples

2.1 LA-ICP-MS analyses

The LA-ICP-MS analyses were carried out at ETH Zürich, using a RESOlution laser ablation system with a 193 nm excimer (ArF) laser source and a two-volume Laurin Technic S-155 ablation cell. To investigate possible matrix effects and the influence of the ablation crater geometry, we used variable crater sizes and repetition rates of the laser, producing laser ablation craters with aspect ratios (crater depth / crater diameter) ranging from 0.08 to 1.3. Crater geometries (depth and diameter) were measured using a Keyence digital microscope VHX-6000.

The ablated aerosol was mixed in the ablation cell with carrier gas consisting of helium ($0.5\,\mathrm{L\,min^{-1}}$) and make-up gas consisting of argon (ca. $1\,\mathrm{L\,min^{-1}}$) and nitrogen ($2\,\mathrm{mL\,min^{-1}}$). The aerosol was then homogenised by a squid smoothing device and introduced into the plasma of the Thermo Element XR ICP-MS. This single collector sector field MS is equipped with a high-capacity ($80\,\mathrm{m^3\,h^{-1}}$) interface pump in combination with jet sampler and normal H-skimmer cones to achieve a detection efficiency in the range of 2 % (based on U in a single spot ablation of NIST SRM612 glass). Detailed instrumentation and data acquisition parameters are summarised in Table A1. A measurement session consists of several samples (20–50-point analyses each), matrix-matched primary RM (WC-1; $n = 20$–40), two validation RMs (ASH-15D (Mason et al., 2013; Vaks et al., 2013) and JT (Jura Thrust); $n = 15$–30) and a homogeneous glass RM (NIST614 or NIST 612; $n = 10$–20). RMs are distributed over the whole sequence to monitor and, if necessary, to correct for instrumental drift.

2.2 LA-ICP-MS data reduction

The data reduction methods largely follow the one described in Roberts et al. (2017) and are described here briefly focusing on differences and some observations. The raw data (time-resolved intensities) from the spectrometer are loaded into the Iolite v.2.5 data reduction software (Paton et al., 2011) and processed using the VisualAge data reduction scheme (Petrus and Kamber, 2012; Paton et al., 2010) to calculate only gas-blank-corrected intensities, raw ratios and their uncertainties. The integration intervals of both reference materials and samples are subsequently adjusted to optimise the spread along the isochron line. The selection of different length or depths for integration intervals for primary RM and the sample or splitting a single spot ablation into several separate intervals can introduce systematic offsets due to different downhole fractionation between the primary RM and the sample. Although best practice would be to use integration intervals that are as identical as possible with respect to a crater shape for both the RM and the sample, the potentially introduced offsets would average out between the different spots for a given sample due to the virtually random distribution of favourable signal intervals (high U, low initial Pb).

Further data reduction including drift and matrix correction uses an in-house spreadsheet based on Microsoft Excel following the protocols in Roberts et al. (2017). The $^{238}U/^{206}Pb$ ratio is drift-corrected using the glass RM, e.g. NIST 614. Due to the low ^{207}Pb count rate on some of the samples and RMs, the $^{207}Pb/^{206}Pb$ ratio is calculated as ratio of the mean count rate for each integration interval and not the mean of the ratios of each sweep. The $^{207}Pb/^{206}Pb$ ratio is corrected for mass bias using the mass bias factor determined from the homogeneous glass RM. The drift-corrected $^{238}U/^{206}Pb$ ratios and the mass bias-corrected $^{207}Pb/^{206}Pb$ ratios of all analyses of the WC-1 calcite RM are subsequently plotted in a Tera–Wasserburg concordia diagram, using IsoplotR (Vermeesch, 2018). An isochron is calculated by linear regression through the resulting data set and anchoring to the initial $^{207}Pb/^{206}Pb$ of 0.85 ± 0.04 (Roberts et al., 2017). The ratio between the lower-intercept age obtained thereby and the reference age of 254.4 ± 6.4 Ma (Roberts et al., 2017) is used as the correction factor for the $^{238}U/^{206}Pb$ ratio

throughout the sequence. This correction factor would encompass matrix effects, including laser-induced (i.e. downhole) element fractionation, and ICP-related U/Pb inter-element fractionation, including mass bias.

2.3 ID-TIMS

For the characterisation of JT as a new potential VRM we used isotope dilution thermal ionisation mass spectrometry methods equivalent to those described in Nuriel et al. (2020). Seven calcite chips of 1.3 to 3.7 mg were sampled from the JT calcite vein using a stainless-steel needle. Individual chips were loaded in 3 mL Savillex beakers and repeatedly cleaned in ultrapure acetone and water. Cleaned aliquots were spiked with 4–8 mg of the EARTHTIME ^{202}Pb–^{205}Pb–^{233}U–^{235}U tracer solution and dissolved in 6N HCl at 120 °C for 30 min. Dissolved samples were dried down and re-dissolved in 1N HBr for anion exchange chromatography. U and Pb were separated using a HBr–HCl-based anion exchange chemistry employing AG1-X8 resin in 50 µL Teflon columns. The U and Pb fractions were collected separately in 7 mL Savillex beakers and dried down with a drop of 0.02 M H_3PO_4. U and Pb were loaded on outgassed Re filaments with a Si-gel ion emitter for thermal ionisation mass spectrometry and analyses were performed using a Thermo TRITON plus instrument at ETH Zürich. Pb isotope ratios were measured on the axial secondary electron multiplier and U was measured as UO_2 employing a static routine with Faraday cups connected to amplifiers with 10^{13} ohm resistors (Wotzlaw et al., 2017). Data reduction and uncertainty propagation was done using Tripoli, an Excel-based spreadsheet that employs algorithms of Schmitz and Schoene (2007) and isochron calculations were performed using IsoplotR (Vermeesch, 2018). U–Pb data were not corrected for ^{234}U and ^{230}Th disequilibria. Uncertainties are reported at the 95 % confidence level without systematic uncertainties associated with tracer calibration and decay constants unless otherwise indicated.

2.4 New validation reference material JT

JT is a vein calcite that originates from a deep borehole in the northern Swiss Molasse Basin and is hosted by a micritic limestone of the Middle Triassic Muschelkalk Group. JT is part of a dense network of calcite veins associated with a thrust fault branching off from the basal décollement of the Jura fold-and-thrust belt (Looser et al., 2020).

3 Results and discussion

All LA-ICP-MS and ID-TIMS data can be found in the Supplement Table S1 (LA-ICP-MS) and Table S2 (ID-TIMS).

3.1 Characterisation of JT as a validation reference material

We characterised the vein calcite JT both by ID-TIMS and LA-ICP-MS (all data provided in the Supplement). The ID-TIMS analyses yielded an isochron, lower-intercept age of 13.797±0.031 Ma ($n = 6$, 1 outlier excluded; MSWD = 3.6), and a $(^{207}Pb/^{206}Pb)_0$ of 0.8394 ± 0.0025 (Fig. 1a). The intercept age of pooled LA-ICP-MS data from 16 sequences with a total of 474 single point analyses (13.75 ± 0.11 Ma or 13.75 ± 0.36 Ma including excess variance ε' – see below; MSWD = 2.0; $(^{207}Pb/^{206}Pb)_0 = 0.8473 \pm 0.008$; Fig. 1b) is identical within uncertainty to the mean of the intercept ages from the same 16 sequences (13.695 ± 0.157 Ma, or 13.70 ± 0.37 Ma including ε'; Fig. 2a). Both overlap well with the ID-TIMS intercept age. Additional measurements of 10 spots on 43 pieces of JT available for distribution show that some pieces are dominated by initial Pb and the overall U concentration ranges from below 0.01 up to 5 µg g^{-1} with a mean of 0.6 ppm and a median of 0.44 µg g^{-1}. The $^{238}U/^{206}Pb$ ratio varies between 0.04 and 455. Detailed description of the results (Table S3) also contain isochrons for each individual piece and can be found in the Supplement.

3.2 Long-term excess variance

The VRMs JT and ASH-15D were analysed 16 and 30 times in 9 and 16 sessions respectively, sometimes with different laser parameters, each yielding an intercept age with uncertainty. Figure 2 shows the sorted intercept ages with uncertainties both without (white) propagation of the long-term (inter-sessions) excess variance (ε') and with propagation (green). The MSWD of the original data sets are 1.57 for JT and 1.26 for ASH-15D. Assuming ideal behaviour of these VRMs (homogeneous age, cogenetic character of all analysed domains and closed system behaviour) an MSWD of ~ 1 is expected. To obtain an MSWD of ~ 1, a long-term (inter-session) excess variance (ε') of 2.5 % (JT) and 2.0 % (ASH-15D) needs to be propagated by quadratic addition to the intercept uncertainty of the individual sequences (Fig. 2). For this calculation, only VRM measurements with a similar aspect ratio to the primary RM were considered. This excess variance is slightly larger than for zircons of ca. 2 % 2S (Horstwood et al., 2016), probably reflecting the difference in age calculation, heterogeneity of RM WC-1 (see Sect. 2.5), heterogeneity of VRMs and matrix differences. The latter two potentially include the selection of integration intervals that do not systematically match those of the primary RM, resulting in slight offsets (see Sect. 1.2).

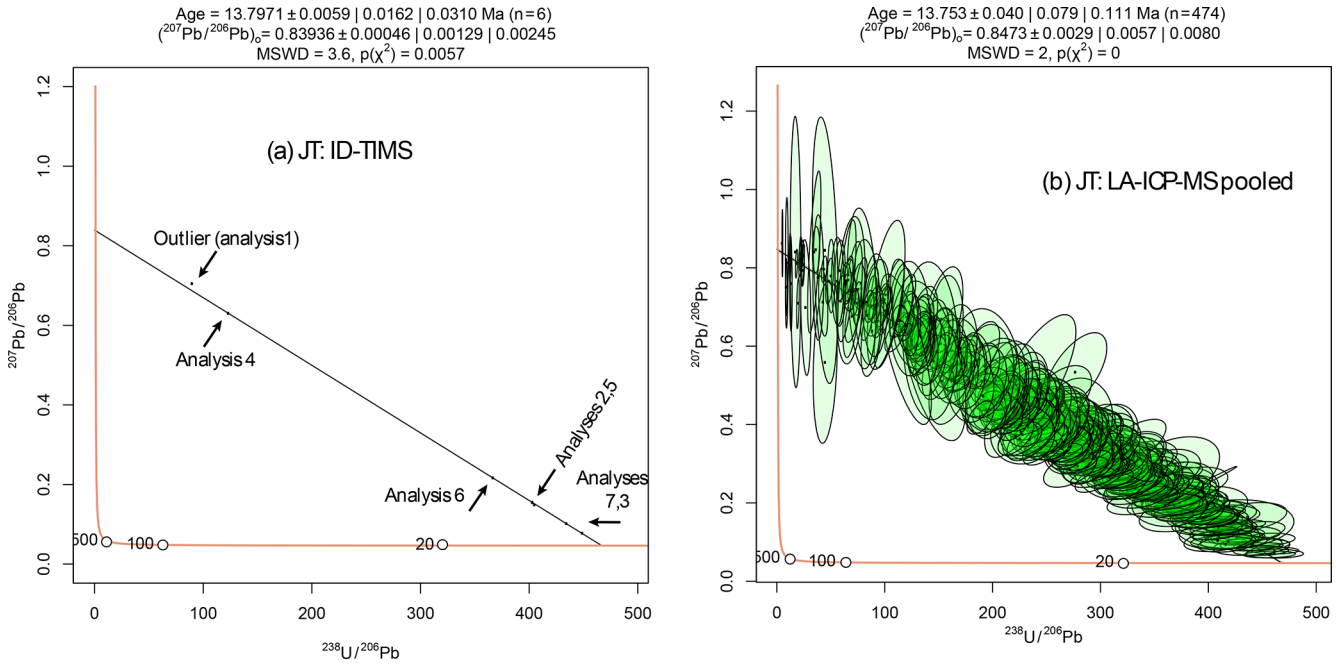

Figure 1. Tera–Wasserburg concordia plot of JT analyses by **(a)** ID-TIMS ($n = 6$) and **(b)** LA-ICP-MS ($n = 474$).

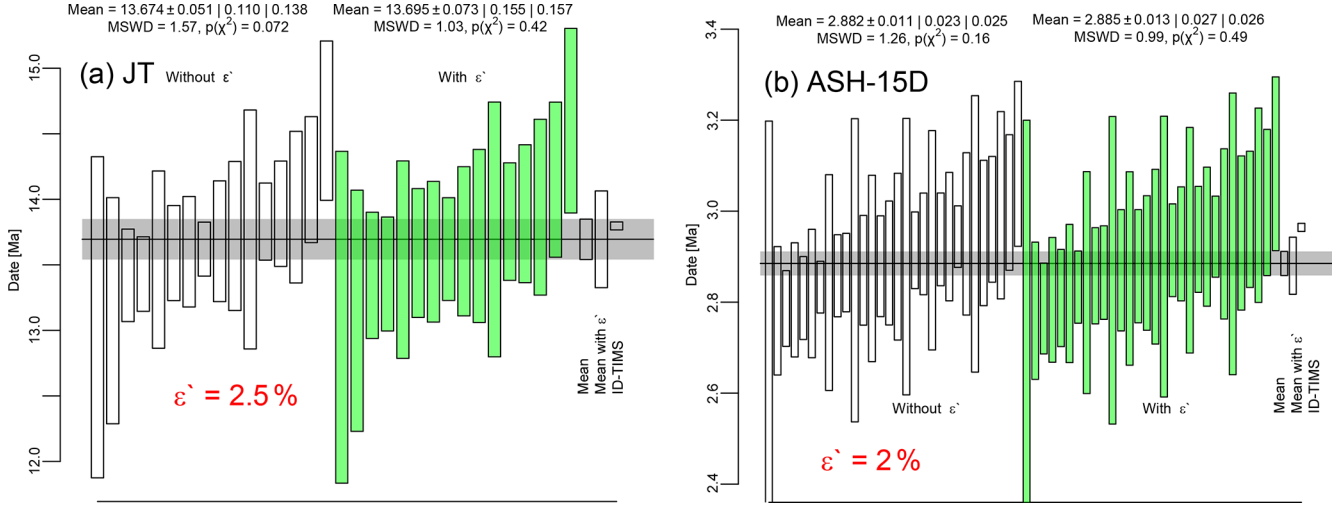

Figure 2. Sorted intercept ages for JT (**a**: white) of $n = 16$ with an MSWD of 1.57 and ASH-15D (**b**: white) of $n = 30$ with an MSWD of 1.26 for the estimation of the long-term excess variance (ε') to be propagated and the same data including ε' (green). Also presented are the super-population mean, mean with ε' and reference age from ID-TIMS. Uncertainties are 95 % confidence levels with overdispersion (white) and 95 % confidence levels with overdispersion and excess long-term variance (green).

3.3 The influence of the ablation crater aspect ratio on data accuracy

3.3.1 Results on tests based on WC-1, JT and ASH-15D

During 15 sequences of carbonate dating, we have measured the validation RM with different crater sizes and repetition rates, matching the need for sufficient signal on the samples with generally low U contents. We varied the crater diameter and repetition rate from 110 µm and 5 Hz for the primary RM WC-1 up to 250 µm and 10 Hz for VRMs and samples (exact parameters are listed for all sessions in Table S1). We first observed that analyses performed with ablation crater diameters larger than those of the primary RM show a systematic offset towards higher $^{238}U/^{206}Pb$ ratios, corresponding to younger isochron intercept ages. This suggests an influence of the crater geometry on the offset between measured and real values, which is problematic when the unknowns and primary

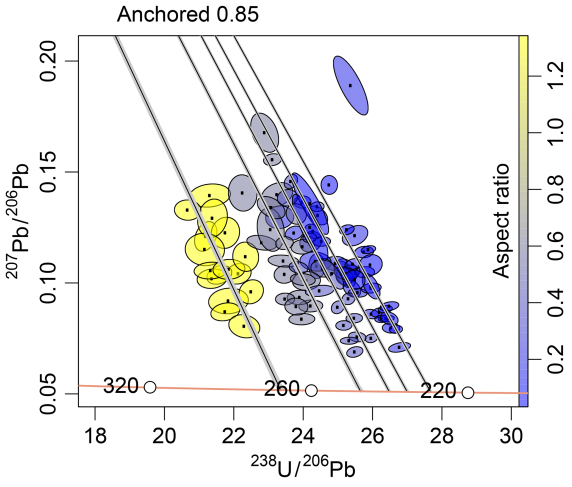

Figure 3. Tera–Wasserburg concordia plot of WC-1 analyses, corrected only for $^{207}Pb/^{206}Pb$ mass bias, ablated with different ablation crater aspect ratios. The deeper the crater, the older the age. Intercept ages are ∼270, 246, 239, 234 and 228 Ma. Ellipses are 95 % confidence level. Individual plots including regression and intercept statistics are shown in Fig. A1.

RM are measured with different crater sizes and/or repetition rates.

Therefore, we further measured a single sequence (190130) analysing WC-1 not only as primary RM with the standard parameters of 110 µm ablation crater diameter and 5 Hz repetition rate, but also with 163 µm, 3 Hz; 110 µm, 10 Hz; 74 µm, 10 Hz; and 51 µm 15 Hz, to systematically investigate the influence of ablation crater aspect ratio. These parameters result in an extreme difference of crater aspect ratios (crater depth / crater diameter) between ∼0.08 (flat crater, 163 µm, 3 Hz) and ∼1.3 (deep crater, 51 µm, 15 Hz). The U–Pb isotopic data, corrected only for $^{207}Pb/^{206}Pb$ mass bias, yield intercept ages between 226 Ma (flat crater) and 267 Ma (deep crater) as shown in Figs. 3 and A1. Plotting the aspect ratio mismatch (armm, aspect ratio of the sample / aspect ratio of the primary RM) vs. the age offset relative to the accepted age, a linear correlation is given not only for WC-1 (Fig. 4a) but also for the validation RM JT (Fig. 4b) and ASH-15D (Fig. 4c).

3.3.2 Variable ablation efficiency for different carbonates

Due to the observed age offset depending on the LA crater geometry (Fig. 4), the ablation rate between RM and unknown sample must be very similar when using identical laser parameters (energy density, crater size and repetition rate) to get the same ablation crater aspect ratio. As the ablation efficiency of an unknown sample is not known prior to ablation, we measured ablation rates of various carbonates with differences in mineralogy (calcite, dolomite, aragonite), crystal size (micritic, sparry), and purity (turbid, clear), relative to the ablation rate of WC-1 (ablation rate of ∼120 nm per laser pulse at energy density of 2 J cm^{-2}) as shown in Fig. 5, to estimate the ablation rate of a "unknown" carbonate. Regardless of their occurrence (i.e. sparry, micritic, etc.), calcite matrices show ablation rates that vary within < 14 % relative to WC-1. In turn, the corresponding armm if WC-1 is used, as the primary RM would result in an offset of the lower-intercept date of 1 % or less (Fig. 4), which is identical to or smaller than the minimum uncertainty on such dates based on our assessment of the excess variance. By contrast, dolomite shows higher ablation efficiencies than calcite and much larger variations, from 105 % to 160 %, relative to WC-1 (Fig. 5). The only aragonite sample tested in this compilation had an even faster ablation rate than dolomite and was almost twice as fast as WC-1 (Fig. 5). We presume that these differences in ablation rates could result in significant age offsets in a roughly estimated range of 4 %–8 % for dolomite (160 % ablation rate compared to WC-1) and 6 %–11 % for aragonite (200 % ablation rate of WC-1) based on the offsets found in Fig. 4. However, this hypothesis needs validation and any attempt to date dolomite or aragonite needs careful validation. In addition, the large spread for dolomite and the small number of tested aragonite samples makes the estimation of the ablation rate unpredictable for these matrices. These results highlight that matrix-matched standardisation is required for accurate LA-ICP-MS U–Pb geochronology of different carbonates and dolomite or aragonite dates obtained using WC-1 calcite as the primary RM might be prone to systematic inaccuracy.

3.3.3 Strategies for matching aspect ratios

The results showed in Fig. 4 suggest that carbonate U–Pb dating by LA-ICP-MS is only accurate when the laser ablation crater aspect ratio is similar between RM and an unknown sample. If the crater geometry varies, an artificial and significant age offset can be introduced (> 10 % relative in extreme cases; Fig. 4). This can be a problem because U contents in carbonates vary by orders of magnitude, while only one characterised RM (WC-1) with relatively homogeneous and high U content (3.7 ± 1 µg g^{-1}, 2 SD; Roberts et al., 2017) is available so far. Therefore, it is not ideal to use one single crater size and repetition rate for all unknowns and RMs. We therefore suggest a two-step strategy to account for this issue: (1) estimate the U content of all unknowns to be dated in a specific sequence, via a short, pre-sequence test run; and (2) apply a crater diameter to each unknown, inversely proportional to its U content, and adjust the repetition rate to match the aspect ratio of the craters in the primary RM. Based on our experience, the test run need not be longer than 0.5 h, with only a few (3–5) spots per sample using a shortened ablation time (10–15 s). Based on this suggestion, it is possible to use larger spot sizes for lower-U samples than used for the RM to improve the counting and precision, as long as the repetition rate is increased accordingly.

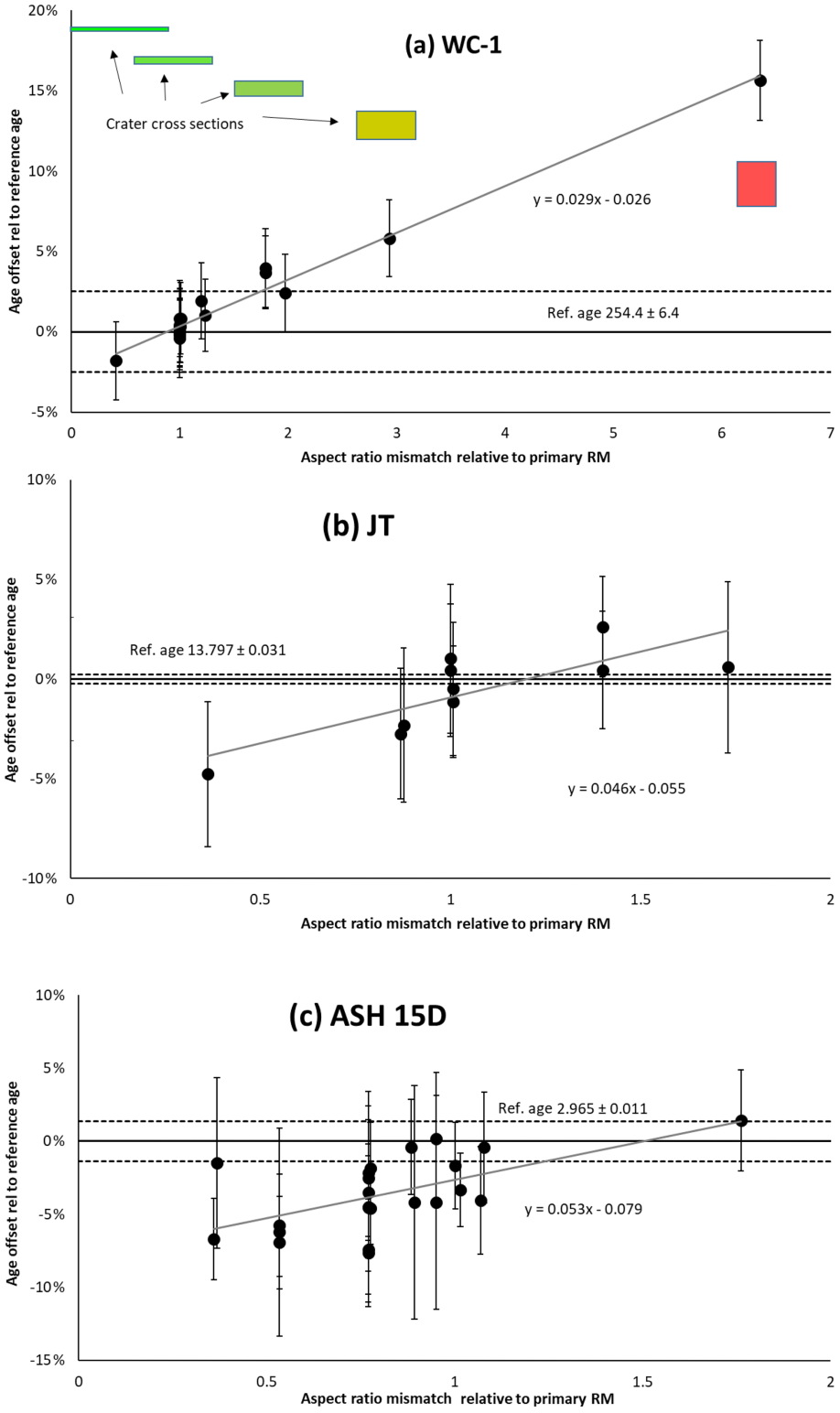

Figure 4. Plots of relative age offsets relative to the accepted age for various calcite RMs as a function of the aspect ratio offset relative to the primary RM. **(a)** WC-1 where the coloured rectangles represent the cross section of the crater (not to scale). **(b)** JT validation RM including the ID-TIMS reference age (this study). **(c)** ASH-15D validation RM including the ID-TIMS reference (Nuriel et al., 2020). Age error bars are 95 % confidence including systematic uncertainties as propagated here (see text for details).

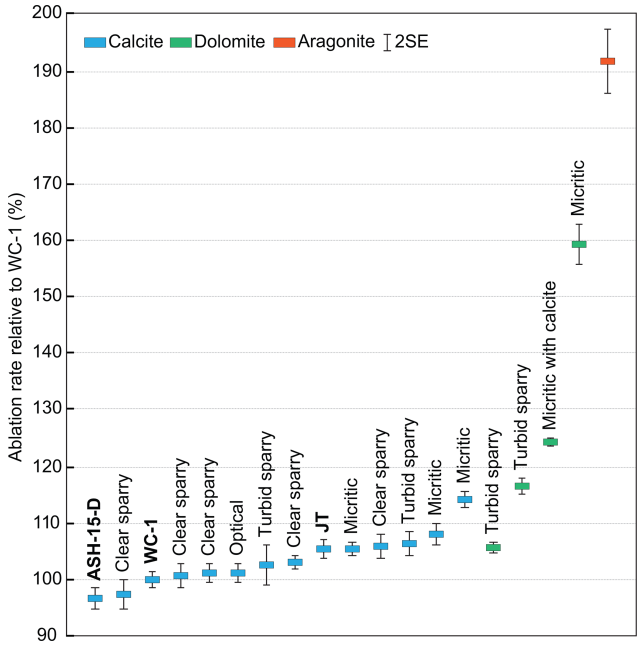

Figure 5. Ablation rate variation relative to WC-1 for different calcite, dolomite and one aragonite sample.

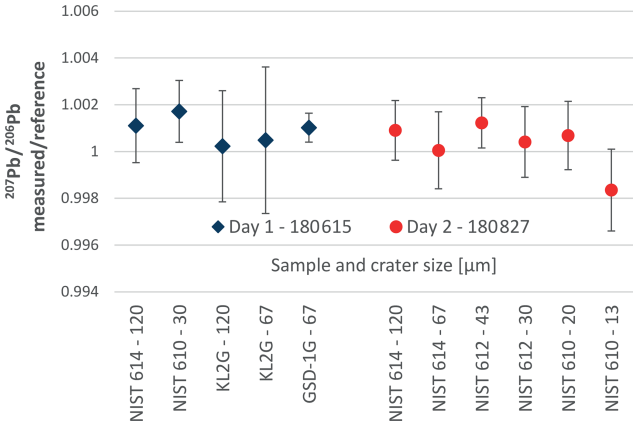

Figure 6. Plot of the ratio between measured and reference $^{207}Pb/^{206}Pb$ ratio in different RM glasses and using different crater sizes. The correction factor shows no variation against RM type or crater size. Error bars are 2 SE.

It is possible to measure the crater depth and aspect ratios of the analysed samples and RMs post ablation and if necessary, apply a correction (based on the linear relationship between aspect ratio mismatch and age offset as shown in Fig. 4) to improve accuracy, especially when dealing with different carbonate minerals. However, this correction will have to be based on measurements with different aspect ratios for both primary and validation RMs ideally within the same session, as it seems likely that both the ablation rate and age offsets are dependent on the actual laser ablation and ICP-MS parameters. A detailed study on how to best apply this correction if necessary is beyond the scope of this work, and we only suggest that for a simpler and more robust data reduction always use similar aspect ratios. As shown in Sect. 2.3.2 and Fig. 5, for various types of calcite the differences in ablation rate relative to WC-1 are sufficiently small for this procedure to lead to accurate ages (i.e. offset by less than 1 % relative).

3.4 $^{207}Pb/^{206}Pb$ correction

NIST 614 has been proposed as an RM for the mass bias correction of the $^{207}Pb/^{206}Pb$ ratio (Roberts et al., 2017) due to the similar Pb concentration to many carbonates. We investigated several homogeneous and well characterised glass RMs (NIST 610, NIST 612, NIST 614, GSD-1G and KL2G) on two different days to be used for this correction, and we found no significant influence from different LA parameters, notably ablation crater diameter and Pb concentration of the RM (Fig. 6). Only the smallest spot size of 13 µm on the highest Pb concentration glass (NIST 610) produced a small offset (within uncertainty) compared to the other glasses.

3.5 WC-1 heterogeneity

We document heterogeneity in the currently most used calcite RM WC-1 (Roberts et al., 2017). This information is meant as a warning to analysts to make sure they understand that carbonates are quite heterogeneous materials and are prone to diagenetic alteration, including open-system processes at various stages in their geological history, resulting in zones with the potential for different ages to be recorded. Care needs to be taken as some WC-1 aliquots may have larger age variation than initially described by Roberts et al. (2017).

To investigate the homogeneity of our aliquot of WC-1, in one sequence (190405) we specifically targeted a brighter, vein-like, more sparry zone, in addition to the normal sampling strategy aiming at the darker, more homogeneous material as shown in Fig. 7. A white alteration vein cross-cutting through the darker zone with a similar appearance to the white zone in our aliquot in the work initially characterising WC-1 (Roberts et al., 2017) was shown to be high in Th and the transition metals. While for that case, no difference in age is documented, our data show that the brighter zones may yield significantly younger ages of 203 ± 7, while the darker zones used for matrix correction in this session yielded the expected results of 254.3 ± 2.2, similar to other sessions and to the results in Roberts et al. (2017). Given the textural difference between the white and the dark calcites, reflecting different ambient conditions during precipitation, the white zone instead reflects precipitation at different times than Pb loss due to open-system behaviour. The analyses of the white zone show a larger scatter than in the dark zones, possibly due to mixing between the two phases in deeper parts of the

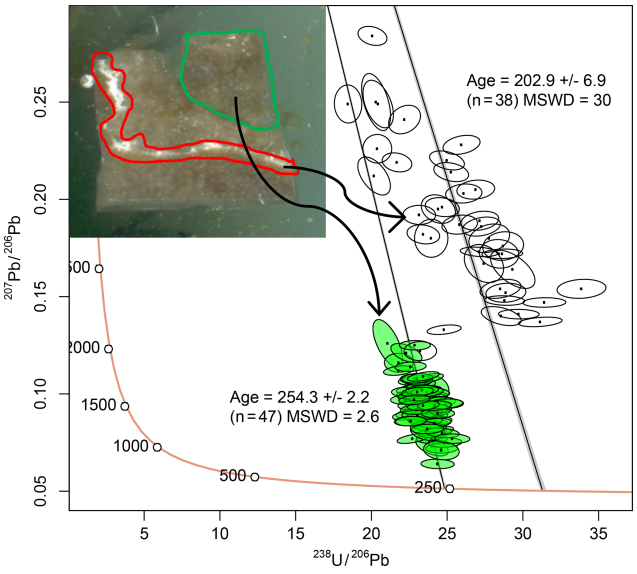

Figure 7. Tera–Wasserburg concordia plot of WC-1 analyses in two different regions of the aliquot fragment as indicated in the inserted image. The darker part (green ellipses) gives results in agreement with the recommended age (254.4 ± 6.4) while the brighter vein-like part (red) gives more scatter and younger ages.

ablation crater. This finding further demonstrates that WC-1 as already described (Roberts et al., 2017) is "not the perfect material because of its modest heterogeneity", not only in chemical composition but also in age. According to our findings, when using WC-1 as RM the locations for analysis have to be chosen carefully and the data have to be screened for outliers to avoid additional scatter and a bias towards younger ages of the RM, finally resulting in older ages for the unknown samples. In particular, points with an increased $^{207}Pb/^{206}Pb$ ratio that fall off from the isochron are potentially biased and should be treated with caution. More generally, this shows that additional and more homogeneous RMs are urgently needed for carbonate dating.

4 Summary and conclusion

We report LA-ICP-MS U–Pb data for previously and newly characterised calcite reference materials. We introduce the JT vein calcite as a potential validation RM due to its homogeneity and very good spread in relative radiogenic to initial Pb contents. The ID-TIMS U–Pb data for JT yielded an isochron intercept date of 13.797 ± 0.031 Ma, consistent with a LA-ICP-MS isochron intercept date of 13.75 ± 0.36 Ma (relative to WC-1).

Repeated LA-ICP-MS analyses of this new VRM and the existing calcite RM ASH-15D over an extended time period show that excess variance of 2 %–2.5 % should be propagated in the individual lower-intercept dates obtained. This estimate of the long-term excess variance is larger than for other LA-ICP-MS geochronological methods such as U–Pb in zircon (Horstwood et al., 2016) and may encompass a greater heterogeneity of samples, primary RM (WC-1) and different ablation rates between both, as highlighted here.

We also document that a mismatch in the ablation crater aspect ratio between the primary RM and unknowns results in significant age offsets. In theory, this offset can be minimised by using the same diameter and repetition rate for standards and unknowns. However, this may not always be possible, especially if the U content is significantly different in unknowns compared to the primary RM, in which case matching the ablation crater aspect ratio of the primary RM is the easiest, most efficient way to get accurate results. For instance, in the case of low U samples, the aspect ratio can be matched by increasing proportionally the laser repetition rate and crater diameter with the other benefit of yielding more signal and thereby decreasing analytical uncertainties. While the correction of the U/Pb ratio is very sensitive to laser ablation parameters, the $^{207}Pb/^{206}Pb$ correction is very insensitive, and it is possible to use almost any well-characterised material with well-characterised Pb isotopic composition.

The offset of 2 %–3 % (usually within the uncertainty) of LA-ICP-MS results for ASH-15D compared to ID-TIMS results remains, while the results for JT are in very good agreement. This offset cannot be explained completely by differences in ablation rate and may be an additional matrix effect to be investigated in detail in future work.

Furthermore, we show differences in ablation rate between different types of calcites (< 14 % relative to WC-1) and, overall, different carbonate minerals (up to $+60$ % for dolomite and up to $+90$ % for aragonite, relative to WC-1). While the expected age offset on calcite is negligible, this likely introduces additional systematic errors that need validation when using non-matrix-matched standardisation, i.e. using WC-1 calcite as a primary RM to date dolomite or aragonite. The latter observation calls for the characterisation of further carbonate standards including various calcites, dolomites and aragonites. This will significantly increase the accuracy and possible applications of carbonate U–Pb geochronology by LA-ICP-MS.

Appendix A: LA-ICP-MS parameters

Table A1. LA-ICP-MS U–(Th–)Pb metadata.

Laboratory and sample preparation	
Laboratory name	Dept of Earth Sciences, ETH Zurich
Sample type/mineral	Carbonates, mostly calcite
Sample preparation	Thin sections or chips mounted in epoxy
Imaging	CL8200 Mk5-2 optical cathodoluminescence system
Laser ablation system	
Make, model and type	ASI (Resonetics) RESOlution S155
Ablation cell and volume	Laurin Technic, two-volume cell, effective volume ca. 1 cm^3
Laser wavelength (nm)	193 nm
Pulse width (ns)	25 ns
Fluence ($J\,cm^{-2}$)	$\sim 1.8\,J\,cm^{-2}$
Repetition rate (Hz)	Variable, see data for actual value
Ablation duration (s)	40 s
Ablation pit depth / ablation rate	Variable, equivalent to 0.09–0.15 µm per pulse
Spot diameter (µm) nominal/actual	Variable, see data for actual value
Sampling mode/pattern	Static spot ablation
Carrier gas	100 % He in the cell, Ar make-up gas combined in cell above ablation in funnel
Cell carrier gas flow ($L\,min^{-1}$)	$0.5\,L\,min^{-1}$
ICP-MS Instrument	
Make, model and type	Thermo Element XR, Sector-field single collector ICP-MS, with high-capacity interface pump
Sample introduction	Ablated aerosol direct
RF power (W)	1350–1550 W (optimised daily)
Make-up gas flow	$0.90–1.05\,L\,min^{-1}$ Ar (optimised daily) $2\,mL\,min^{-1}$ N_2
Detection system	Triple (pulse-counting, analogue, Faraday) cross-calibrated daily with U 238, fixed analogue counting factor (ACF) value, all isotopes usually in pulse-counting only (< 5 Mcps)
Masses measured (amu)	202, 204, 206, 207, 208, 232, 235, 238
Integration time per peak/dwell times (ms)	11 ms (all masses) except: 206, 207 (50 ms)
Total integration time per output data point (s)	0.174 s
Sensitivity/efficiency (%, element)	~ 1 % U
Dead time (ns)	25
Typical oxide rate (ThO / Th)	0.18 %
Typical doubly charged rate (Ba^{++}/Ba^{+})	3.50 %

Table A1. Continued.

Data processing	
Gas blank	20 s
Calibration strategy	NIST614 glass standard as primary reference material for drift and Pb–Pb ratios; WC-1 carbonate standard for matrix matching of $^{206}Pb/^{238}U$; ASH-15-D and JT carbonate for quality control
Reference material info	NIST614 (concentration data: Jochum et al. 2011; Pb isotopes: Baker et al. 2004); WC-1 (Roberts et al., 2017); ASH-15-D (Nuriel et al., 2020); JT (characterised in this work)
Data processing package used	Iolite 2.5, VisualAge for integration, interval selection and gas blank correction only. In-house spreadsheet data processing. IsoplotR (Vermeesch 2018) for isochrons, intercept ages and initial Pb compositions
Correction for LIEF	No LIEF correction (ratio of mean intensities $^{207}Pb/^{206}Pb$ or mean of uncorrected ratios $^{238}U/^{206}Pb$ used)
Mass discrimination	Normalised to reference material (sample standard bracketing)
Common-Pb correction, composition and uncertainty	None applied; ages calculated from regressions in Tera–Wasserburg concordia plots.
Uncertainty level and propagation	Intercept ages are quoted at 2s absolute; propagation is by quadratic addition. Counting statistics uncertainty are propagated to the $^{207}Pb/^{206}Pb$ ratio, together with the uncertainty of the RM value and the uncertainty of repeated measurements. The uncertainty value for lower-intercept isochron ages includes uncertainties from the RM and asystematic uncertainties, estimated in this work to be 2.5 %. Decay constant uncertainties are neglected.
Quality control/validation	ASH 15D: mean of $^{206}Pb/^{238}U$ intercept ages: 2.885 ± 0.076 Ma (2s, MSWD = 0.99, $n = 30$) (0.9 % weighted average uncertainty (internal), 2.0 % total external uncert.)
	JT – mean of $^{206}Pb/^{238}U$ intercept ages: 13.70 ± 0.37 Ma (2s, MSWD = 1.03, $n = 16$) (1.15 % weighted average uncertainty (internal), 2.5 % total external uncert.)
	Systematic uncertainty for propagation is 2.5 % (2s)

This reporting is based on a template available for download at http://www.plasmage.org/ (last access: 24 June 2020).

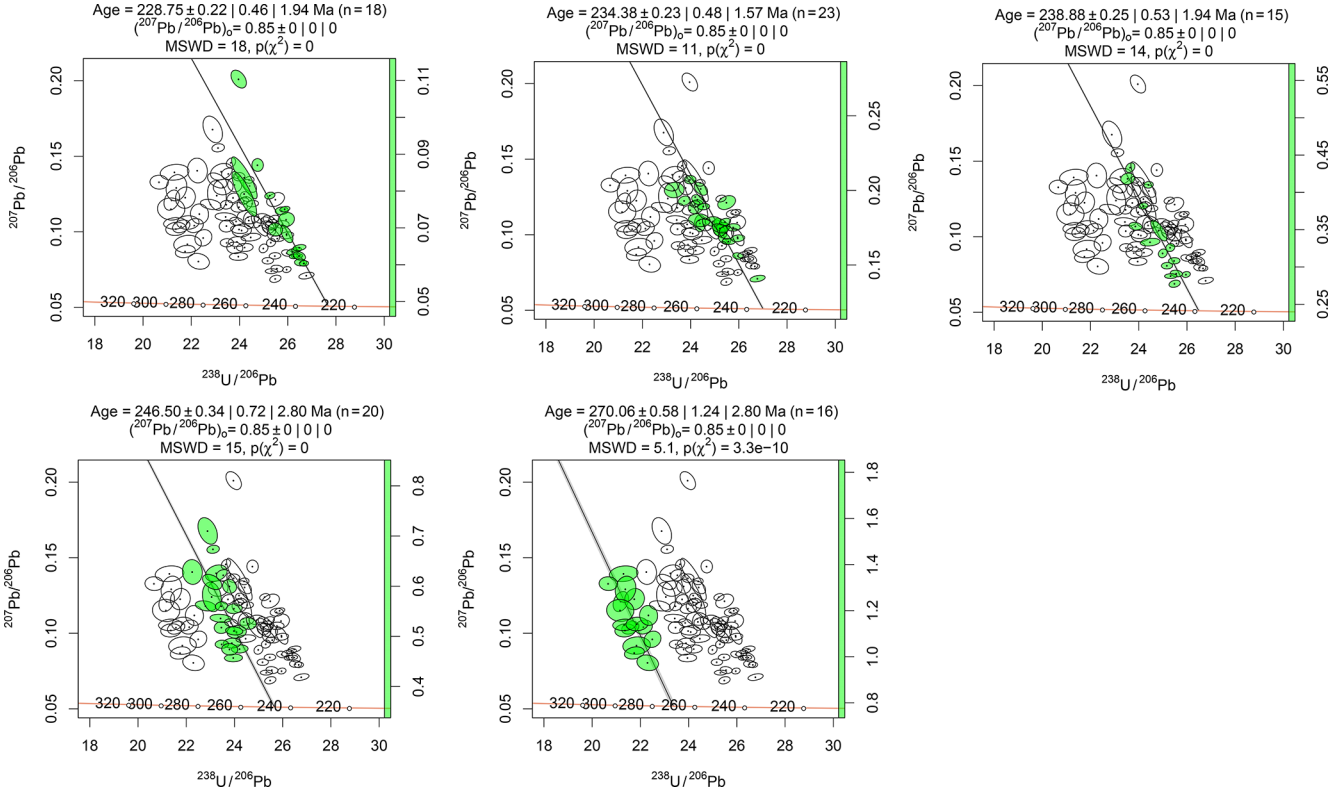

Figure A1. Intercept statistics of Fig. 2. WC-1 analysed with different aspect ratios.

Data availability. All data used in this paper are available from the files in the Supplement.

Sample availability. Sample JT is available on request in limited quantities from the author: guillong@erdw.ethz.ch.

Supplement. The supplement related to this article is available online at: https://doi.org/10.5194/gchron-2-155-2020-supplement.

Author contributions. MG adapted the LA-ICP-MS methodology and data reduction, designed the LA experiments, carried out most measurements, and wrote the paper with input from all coauthors. JFW did the ID-TIMS measurements of JT. NL provided the RM JT, prepared the samples, and did some LA-ICP-MS and most of the ablation rate measurements. OL did some LA-ICP-MS measurements and was involved in the adaption of the methodology, data reduction process and quality control.

Special issue statement. This article is part of the special issue "In situ carbonate U–Pb geochronology". It is a result of the Goldschmidt conference, Barcelona, Spain, 18–23 August 2019.

Acknowledgements. Olivier Bachman and Stefano M. Bernasconi are acknowledged supporting this work. Perach Nuriel is acknowledged for RM ASH-15D, Nick Roberts is acknowledged for RM WC-1. Critical reading and comments by Andrew R. Kylander-Clark, David M. Chew and Nick Roberts helped to improve the paper.

Review statement. This paper was edited by Axel Gerdes and reviewed by David M. Chew and Andrew R. Kylander-Clark.

References

Beaudoin, N., Lacombe, O., Roberts, N. M. W., and Koehn, D.: U-Pb dating of calcite veins reveals complex stress evolution and thrust sequence in the Bighorn Basin, Wyoming, USA, Geology, 46, 1015–1018, 10.1130/g45379.1, 2018.

Burisch, M., Gerdes, A., Walter, B. F., Neumann, U., Fettel, M., and Markl, G.: Methane and the origin of five-element veins: Mineralogy, age, fluid inclusion chemistry and ore forming processes in the Odenwald, SW Germany, Ore Geol. Rev., 81, 42–61, https://doi.org/10.1016/j.oregeorev.2016.10.033, 2017.

Burisch, M., Walter, B. F., Gerdes, A., Lanz, M., and Markl, G.: Late-stage anhydrite-gypsum-siderite-dolomite-calcite assemblages record the transition from a deep to a shallow hydrothermal system in the Schwarzwald mining district, SW Germany, Geochim. Cosmochim. Acta, 223, 259–278, https://doi.org/10.1016/j.gca.2017.12.002, 2018.

Coogan, L. A., Parrish, R. R., and Roberts, N. M. W.: Early hydrothermal carbon uptake by the upper oceanic crust: Insight from in situ U-Pb dating, Geology, 44, 147–150, https://doi.org/10.1130/g37212.1, 2016.

Drake, H., Heim, C., Roberts, N. M. W., Zack, T., Tillberg, M., Broman, C., Ivarsson, M., Whitehouse, M. J., and Astrom, M. E.: Isotopic evidence for microbial production and consumption of methane in the upper continental crust throughout the Phanerozoic eon, Earth Planet. Sc. Lett., 470, 108–118, https://doi.org/10.1016/j.epsl.2017.04.034, 2017.

Drost, K., Chew, D., Petrus, J. A., Scholze, F., Woodhead, J. D., Schneider, J. W., and Harper, D. A. T.: An Image Mapping Approach to U-Pb LA-ICP-MS Carbonate Dating and Applications to Direct Dating of Carbonate Sedimentation, Geochem. Geophy. Geosy., 19, 4631–4648, https://doi.org/10.1029/2018gc007850, 2018.

Godeau, N., Deschamps, P., Guihou, A., Leonide, P., Tendil, A., Gerdes, A., Hamelin, B., and Girard, J. P.: U-Pb dating of calcite cement and diagenetic history in microporous carbonate reservoirs: Case of the Urgonian Limestone, France, Geology, 46, 247–250, https://doi.org/10.1130/g39905.1, 2018.

Goodfellow, B. W., Viola, G., Bingen, B., Nuriel, P., and Kylander-Clark, A. R. C.: Palaeocene faulting in SE Sweden from U-Pb dating of slickenfibre calcite, Terra Nova, 29, 321–328, https://doi.org/10.1111/ter.12280, 2017.

Guillong, M., von Quadt, A., Sakata, S., Peytcheva, I., and Bachmann, O.: LA-ICP-MS Pb-U dating of young zircons from the Kos-Nisyros volcanic centre, SE Aegean arc, J. Anal. Atom. Spectrom., 29, 963–970, https://doi.org/10.1039/c4ja00009a, 2014.

Hellwig, A., Voigt, S., Mulch, A., Frisch, K., Bartenstein, A., Pross, J., Gerdes, A., and Voigt, T.: Late Oligocene to early Miocene humidity change recorded in terrestrial sequences in the Ili Basin (south-eastern Kazakhstan, Central Asia), Sedimentology, 65, 517–539, https://doi.org/10.1111/sed.12390, 2018.

Horstwood, M. S., Košler, J., Gehrels, G., Jackson, S. E., McLean, N. M., Paton, C., Pearson, N. J., Sircombe, K., Sylvester, P., and Vermeesch, P.: Community-Derived Standards for LA-ICP-MS U-(Th-) Pb Geochronology–Uncertainty Propagation, Age Interpretation and Data Reporting, Geostand. Geoanal. Res., 40, 311–332, https://doi.org/10.1111/j.1751-908X.2016.00379.x, 2016.

Li, Q., Parrish, R. R., Horstwood, M. S. A., and McArthur, J. M.: U-Pb dating of cements in Mesozoic ammonites, Chem. Geol., 376, 76–83, https://doi.org/10.1016/j.chemgeo.2014.03.020, 2014.

Looser, N., Madritsch, H., Guillong, M., Laurent, O., Wohlwend, S., and Bernasconi, S. M.: Constraining tectonic activity of the Jura fold-and-thrust belt's basal decollement with U-Pb dating and clumped isotope thermometry, in preparation, 2020.

MacDonald, J. M., Faithfull, J. W., Roberts, N. M. W., Davies, A. J., Holdsworth, C. M., Newton, M., Williamson, S., Boyce, A., and John, C. M.: Clumped-isotope palaeothermometry and LA-ICP-MS U-Pb dating of lava-pile hydrothermal calcite veins, Contrib. Mineral. Petr., 174, 63, https://doi.org/10.1007/s00410-019-1599-x, 2019.

Mason, A. J., Henderson, G. M., and Vaks, A.: An Acetic Acid-Based Extraction Protocol for the Recovery of U, Th and Pb from Calcium Carbonates for U-(Th)-Pb Geochronology, Geostand. Geoanal. Res., 37, 261–275, https://doi.org/10.1111/j.1751-908X.2013.00219.x, 2013.

Methner, K., Mulch, A., Fiebig, J., Wacker, U., Gerdes, A., Graham, S. A., and Chamberlain, C. P.: Rapid Middle Eocene temperature

change in western North America, Earth Planet. Sc. Lett., 450, 132–139, https://doi.org/10.1016/j.epsl.2016.05.053, 2016.

Nuriel, P., Weinberger, R., Kylander-Clark, A. R. C., Hacker, B. R., and Craddock, J. P.: The onset of the Dead Sea transform based on calcite age-strain analyses, Geology, 45, 587–590, https://doi.org/10.1130/g38903.1, 2017.

Nuriel, P., Wotzlaw, J. F., Ovtcharova, M., Stremtan, C., Sala, M., Roberts, N. M. W., and Kylander-Clark, A. R. C.: The use of ASH15 flowstone as matrix-matched standard for laser-ablation U-Pb geochronology of calcite, Geochronology, in preparation, 2020.

Paton, C., Woodhead, J. D., Hellstrom, J. C., Hergt, J. M., Greig, A., and Maas, R.: Improved laser ablation U-Pb zircon geochronology through robust downhole fractionation correction, Geochem. Geophy. Geosy., 11, Q0AA06, https://doi.org/10.1029/2009gc002618, 2010.

Paton, C., Hellstrom, J., Paul, B., Woodhead, J., and Hergt, J.: Iolite: Freeware for the visualisation and processing of mass spectrometric data, J. Anal. Atom. Spectrom., 26, 2508–2518, 10.1039/c1ja10172b, 2011.

Petrus, J. A. and Kamber, B. S.: VizualAge: A Novel Approach to Laser Ablation ICP-MS U-Pb Geochronology Data Reduction, Geostand. Geoanal. Res., 36, 247–270, https://doi.org/10.1111/j.1751-908X.2012.00158.x, 2012.

Roberts, N. M. W. and Walker, R. J.: U-Pb geochronology of calcite-mineralized faults: Absolute timing of rift-related fault events on the northeast Atlantic margin, Geology, 44, 531–534, https://doi.org/10.1130/g37868.1, 2016.

Roberts, N. M. W., Rasbury, E. T., Parrish, R. R., Smith, C. J., Horstwood, M. S. A., and Condon, D. J.: A calcite reference material for LA-ICP-MS U-Pb geochronology, Geochem. Geophys. Geosy., 18, 2807–2814, https://doi.org/10.1002/2016gc006784, 2017.

Scardia, G., Parenti, F., Miggins, D. P., Gerdes, A., Araujo, A. G. M., and Neves, W. A.: Chronologic constraints on hominin dispersal outside Africa since 2.48 Ma from the Zarqa Valley, Jordan, Quaternary Sci. Rev., 219, 1–19, https://doi.org/10.1016/j.quascirev.2019.06.007, 2019.

Schmitz, M. D. and Schoene, B.: Derivation of isotope ratios, errors, and error correlations for U-Pb geochronology using Pb-205-U-235-(U-233)-spiked isotope dilution thermal ionization mass spectrometric data, Geochem. Geophy. Geosy., 8, Q08006, https://doi.org/10.1029/2006gc001492, 2007.

Vaks, A., Woodhead, J., Bar-Matthews, M., Ayalon, A., Cliff, R. A., Zilberman, T., Matthews, A., and Frumkin, A.: Pliocene-Pleistocene climate of the northern margin of Saharan-Arabian Desert recorded in speleothems from the Negev Desert, Israel, Earth Planet. Sc. Lett., 368, 88–100, https://doi.org/10.1016/j.epsl.2013.02.027, 2013.

Vermeesch, P.: IsoplotR: A free and open toolbox for geochronology, Geosci. Front., 9, 1479–1493, https://doi.org/10.1016/j.gsf.2018.04.001, 2018.

Walter, B. F., Gerdes, A., Kleinhanns, I. C., Dunkl, I., von Eynatten, H., Kreissl, S., and Markl, G.: The connection between hydrothermal fluids, mineralization, tectonics and magmatism in a continental rift setting: Fluorite Sm-Nd and hematite and carbonates U-Pb geochronology from the Rhinegraben in SW Germany, Geochim. Cosmochim. Acta, 240, 11–42, https://doi.org/10.1016/j.gca.2018.08.012, 2018.

Wotzlaw, J. F., Buret, Y., Large, S. J. E., Szymanowski, D., and von Quadt, A.: ID-TIMS U-Pb geochronology at the 0.1 parts per thousand level using 10(13) Omega resistors and simultaneous U and O-18/O-16 isotope ratio determination for accurate UO2 interference correction, J. Anal. Atom. Spectrom., 32, 579–586, https://doi.org/10.1039/c6ja00278a, 2017.

Yokoyama, T., Kimura, J. I., Mitsuguchi, T., Danhara, T., Hirata, T., Sakata, S., Iwano, H., Maruyama, S., Chang, Q., Miyazaki, T., Murakami, H., and Saito-Kokubu, Y.: U-Pb dating of calcite using LA-ICP-MS: Instrumental setup for non-matrix-matched age dating and determination of analytical areas using elemental imaging, Geochem. J., 52, 531–540, https://doi.org/10.2343/geochemj.2.0541, 2018.